Jurica Sorić
Josip Hoster
Tomislav Jarak
Boris Jalušić

ISSN 1333-11243
eISSN 1849-1391

MIXED MESHLESS PLATE ANALYSIS USING B-SPLINE INTERPOLATION

Summary

A new mixed meshless approach using the interpolation of both stress and displacement has been proposed for the analysis of plate deformation responses. Kinematic of a three dimensional solid is adopted and discretization is performed by nodes located on the upper and lower plate surfaces. Governing equations are derived by employing the local Petrov-Galerkin approach. The approximation of all unknown field variables is carried out by using the B-spline interpolation and the moving least squares functions in the in-plane directions, while linear polynomials are applied in the transversal direction. In order to eliminate the thickness locking effect, the hierarchical quadratic interpolation of the transversal displacement component through the thickness is used. The shear locking effect is efficiently suppressed by the interpolation of the stress field independently from the displacement. The numerical efficiency of the derived algorithm is demonstrated by numerical examples.

Key words: *mixed meshless approach, plates, B-spline interpolation, shear locking, thickness locking*

1. Introduction

In recent years, numerical approaches known as meshless methods have attracted considerable attention due to their potential to overcome shortcomings associated with mesh-based numerical methods, such as the Finite Element Method (FEM). Using these numerical procedures, a computational model may be discretized only by nodes which do not need to be connected into elements. Thus, some issues associated with the FEM, such as a time-consuming mesh generation or element distortion problems, may be efficiently overcome by using meshless formulations.

In addition, the meshless methods can also successfully deal with various locking phenomena which usually appear in the thin plate and shell analysis. Therefore, a number of different meshless formulations have been proposed. However, some of these approaches still require certain meshes in the form of background cells to integrate weak forms, as can be found in the Element-Free Galerkin (EFG) method [1, 2]. On the contrary, the Meshless Local Petrov-Galerkin (MLPG) method [3] does not require any kind of element mesh for either interpolation or integration and therefore represents a truly meshless approach. The MLPG

method has already been successfully applied for solving various problems dealing with shell-like structures, such as the elasto-statics of homogenous plates [4], the analysis of composite plates [5] or the elasto-dynamics of plate structures [6, 7]. Furthermore, the MLPG formulations for the analysis of shear-deformable shells [8, 9] have also been developed. All those formulations are mainly based on some of classical theories, e.g. the Kirchhoff-Love theory or the Reissner-Mindlin theory. The common drawback of such approaches is that they do not allow a direct implementation of general three-dimensional (3-D) material laws, which may be important in the modelling of shell-like structural components, especially in the case of material nonlinearities.

The MLPG formulations employing a 3-D solid concept are proposed in [10, 11] for plate analyses, and their application to shells is presented in [12]. Therein, the in-plane interpolation has been performed by using the standard Moving Least Squares (MLS) approximation. The hierarchical quadratic interpolation through the thickness has been applied for the transversal displacement component in order to eliminate the undesired thickness locking effect. Like in the most formulations using the Reissner-Mindlin approach mentioned above, the shear locking phenomena in the thin structural limit is only minimized [12] by applying the displacement interpolation functions of a sufficiently high order. On the other hand, the same locking effect is alleviated in [11] by introducing new field variables such as the transversal shear strains and some special displacement variables.

A mixed formulation based on the interpolation of the strain and the displacement fields has been proposed in [13] for plate analyses. In this approach, the thickness and shear locking phenomena are efficiently eliminated by a proper approximation of the strain components. In contrast to the standard fully displacement MLPG approaches, low-order MLS functions are used, which significantly contributes to accuracy and numerical efficiency. Besides the displacement vector interpolation, the independent approximation of the strain tensor components and the transversal normal stress components are proposed in [14]. Herein, the interpolation of the transversal shear strain components yields the shear locking elimination, while the thickness locking is suppressed by means of the transversal normal stress component distribution. The interpolation has been performed by using the modified MLS shape function proposed in [15, 16], that obeys the interpolation condition with high accuracy. It has been demonstrated that the proposed mixed formulation is computationally superior to the fully displacement MLPG approach considered in [12]. However, it is to note that the above mentioned mixed formulations require relatively complex transformation procedures, and moreover, it is well known that the derivation of the MLS shape functions, often applied in meshless analyses, is connected with the complex mathematical approaches.

In the present contribution, besides the MLS interpolation procedures, the B-spline shape function is proposed for the first time for the meshless analysis of plate structures. Instead of the strain and the stress interpolations mentioned above, here only the stress approximation is combined with the displacement distribution. The formulation presented is again based on the concept of a 3-D solid, allowing the implementation of complete 3-D material models. Discretization is performed by nodes located on the upper and lower surfaces, and the local weak form of the equilibrium over the prismatic local sub-domain, surrounding the couple of nodes positioned on the opposite surfaces, is derived. By analogy to the computational strategy presented in [13, 14], the nodal stress values are eliminated locally using the displacement interpolation by means of a collocation approach. Since the B-spline shape function is not interpolatory, a linear transformation of nodal values is performed in order to impose the interpolatory condition. The delta property of the MLS function is enforced by its modification, like in [14]. The stress components interpolation contributes to the shear locking elimination, and the thickness locking is suppressed by using the hierarchical quadratic interpolation of the

transversal displacement components through the thickness. All comments regarding the advantage of the mixed computational strategy over the standard fully displacement formulations quoted in [13, 14] also hold for the formulation presented in this contribution. The performance of the proposed formulation is demonstrated by numerical examples.

The paper is organized as follows: Section 2 presents the derivation of the governing equations for the plate analysis based on the MLPG mixed approach. The discretization procedure with the description of the MLS and B-spline interpolations is presented in Section 3. The numerical examples demonstrating robustness and accuracy of the proposed computational strategy are presented in Section 4. The concluding remarks are given in Section 5.

2. MLPG mixed approach for plate analysis

In order to derive the governing equations for the proposed formulation, a homogeneous plate of uniform thickness is considered. The 3-D Cartesian co-ordinate system with the X^1-X^2 plane lying on the plate middle surface is used, as shown in Fig. 1.

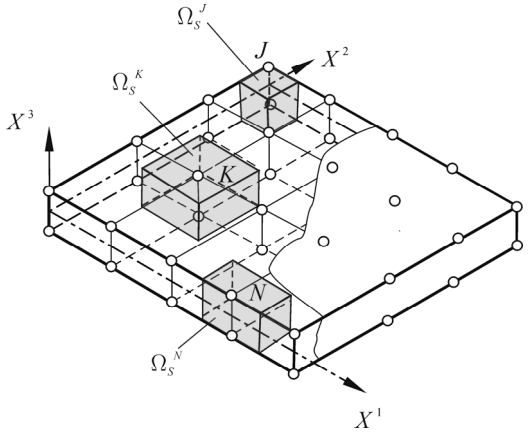

Fig. 1 Discretization of plate continuum

The well-known equilibrium equations referring to such coordinate system may be written for a global 3-D plate domain Ω bounded by a global surface Γ as

$$\sigma_{ij,j} + b_i = 0, \text{ in}\,\Omega, \tag{1}$$

where σ_{ij} is the stress tensor and b_i denotes the body force vector. On the surface Γ, the following boundary conditions are given:

$$u_i = \overline{u}_i, \text{ on}\,\Gamma_u, \tag{2}$$

$$t_i = \sigma_{ij} n_j = \overline{t}_i, \text{on}\,\Gamma_t. \tag{3}$$

Herein, Γ_u and Γ_t are the parts of the global boundary Γ with the prescribed displacements $\overline{u}_i$ and tractions $\overline{t}_i$, respectively. n_j denotes direction cosines of the outward normal vector on Γ.

The plate continuum is discretized by a set of node couples, where the nodes are positioned on the upper and lower plate surface as shown in Fig. 1. According to the Local Petrov-Galerkin approach [3], the equilibrium equations (1) may be written in a weak form over the local sub-domain Ω_s^I, surrounding the I^{th} node couple and bounded by the local boundary surface $\partial\Omega_s^I$, as

$$\int_{\Omega_s^I} \left(\sigma_{ij,j} + b_i\right) v_{ki}\, \mathrm{d}\Omega = 0;\ I = 1,2,...,N, \tag{4}$$

where N stands for the total number of the node couples used for the plate discretization. v_{ki} represents the applied test functions. It is to note that Ω_s^I could theoretically be of any geometric shape and size. Furthermore, according to the Petrov-Galerkin principle, the test and trial functions may be taken from different functional spaces. According to [17], the test functions are chosen as $v_{ik} = \delta_{ik} v$, where v is a kinematically admissible test function and δ_{ik} denotes the Kronecker delta. In the present contribution, the prismatic local sub-domains as shown in Fig. 1 are used and v is assumed to be linear over the plate thickness

$$v\left(X^3\right) = c_0\left(\frac{1}{2} - \frac{X^3}{h}\right) + c_1\left(\frac{1}{2} + \frac{X^3}{h}\right) \tag{5}$$

with c_0 and c_1 as arbitrary real constants and h stands for the plate thickness.

By inserting Eq. (5) in Eq. (4), using the divergence theorem and taking $t_i = n_j \sigma_{ij}$ on $\partial\Omega_s^I$ into account, the following system of the governing equations for the local sub-domain Ω_s^I is derived

$$\begin{aligned}
&\int_{\Omega_s^I} \alpha\left(X^3\right)_{,j} \sigma_{ij}\, \mathrm{d}\Omega - \int_{L_s^I} \alpha\left(X^3\right) n_j \sigma_{ij}\, \mathrm{d}\Gamma - \int_{\Gamma_{su}^I} \alpha\left(X^3\right) n_j \sigma_{ij}\, \mathrm{d}\Gamma = \\
&\qquad = \int_{\Omega_s^I} \alpha\left(X^3\right) b_i\, \mathrm{d}\Omega + \int_{\Gamma_{st}^I} \alpha\left(X^3\right) \overline{t}_i\, \mathrm{d}\Gamma \\
&\int_{\Omega_s^I} \beta\left(X^3\right)_{,j} \sigma_{ij}\, \mathrm{d}\Omega - \int_{L_s^I} \beta\left(X^3\right) n_j \sigma_{ij}\, \mathrm{d}\Gamma - \int_{\Gamma_{su}^I} \beta\left(X^3\right) n_j \sigma_{ij}\, \mathrm{d}\Gamma = \\
&\qquad = \int_{\Omega_s^I} \beta\left(X^3\right) b_i\, \mathrm{d}\Omega + \int_{\Gamma_{st}^I} \beta\left(X^3\right) \overline{t}_i\, \mathrm{d}\Gamma \\
&I = 1, 2, ..., N,
\end{aligned} \tag{6}$$

where

$$\alpha\left(X^3\right) = \left(\frac{1}{2} - \frac{X^3}{h}\right), \quad \beta\left(X^3\right) = \left(\frac{1}{2} + \frac{X^3}{h}\right). \tag{7}$$

Herein, the stress tensor components σ_{ij} are approximated independently from displacements as explained in the following section. As evident, the local boundary $\partial\Omega_s^I$ is divided into three parts, $\partial\Omega_s^I = L_s^I \cup \Gamma_{st}^I \cup \Gamma_{su}^I$, where L_s^I is the part of $\partial\Omega_s^I$ inside the global domain Ω, while Γ_{st}^I and Γ_{su}^I coincide with the parts of Γ with the prescribed natural and essential boundary conditions, respectively. The linear distribution of the in-plane and transversal normal stress components over the plate thickness is assumed, while the transversal shear stress components are constant.

3. Discretization

3.1 MLS interpolation

Since the MLS interpolation is well-known in the meshless formulations, see e.g. [3, 18], it will be presented here very briefly. The MLS nodal shape function $\phi^J\left(X^\delta\right)$ is defined as

$$\phi^J\left(X^\delta\right)=\sum_{i=1}^{m}p_i(\bar{X}^\delta)\left[\mathbf{A}^{-1}\mathbf{B}\right]_{iJ}\,, \tag{8}$$

with **A** as a momentum matrix

$$\mathbf{A}=\sum_{J=1}^{n}W_J(X^\delta)\mathbf{p}(\bar{X}_J^\delta)\mathbf{p}^T(\bar{X}_J^\delta)\,, \tag{9}$$

and the matrix **B** defined as

$$\begin{aligned}\mathbf{B}=\Big[&W_1(X^\delta)\,\mathbf{p}(\bar{X}_1^\delta)\quad W_2(X^\delta)\,\mathbf{p}(\bar{X}_2^\delta)\quad\cdots\\&\cdots\quad W_J(X^\delta)\,\mathbf{p}(\bar{X}_J^\delta)\quad\cdots\quad W_n(X^\delta)\,\mathbf{p}(\bar{X}_n^\delta)\Big].\end{aligned} \tag{10}$$

The complete monomial basis $\mathbf{p}\left(\bar{X}^\delta\right)$ is expressed in terms of the local normalized coordinates in the middle surface directions $\bar{X}^\delta$ in order to improve the conditioning of the matrix **A**, as explained in [12]. $W_J(X^\delta)$ is the weight function associated with the J^{th} node couple. Herein, a regularized weight function, similar to those in [15, 16], is employed to ensure a sufficiently accurate enforcement of the Kronecker delta property, which leads to the same condition for the MLS shape function, i.e. $\phi_J\left(X_I^\delta\right)\approx\delta_{JI}$.

3.2 B-spline interpolation

B-spline interpolations have a wide application in engineering. They are mostly used in surface generation in the geometric modelling of a computer aided design system. B-spline functions may also be employed as interpolating functions to solve structural problems as reported in [19], where they are used in FEM formulations. The recently proposed Isogeometric Analysis is based on the Non-Uniform Rational B-Splines (NURBS), which are used for both the geometry and field approximation [20]. In the present contribution, the B-spline is used as the interpolation function in the frame of the MLPG meshless method.

Here, the derivation of the two-dimensional (2-D) B-spline shape function is summarized. We start with the definition of the B-spline curve which is defined by the following expression

$$C(x)=\sum_{i=1}^{n}N_{i,p}(x)\,P_i\,, \tag{11}$$

where $N_{i,p}(x)$ are the B-spline basis functions of order p and P_i are their coefficients referred to as control points. In general, the control points are not interpolated by B-spline curves. The basis functions are formed by the knot vector $\mathbf{X}_k=\left[x_1\quad x_2\quad\cdots\quad x_{n+p+1}\right]$, which specifies the distribution of parameter x along the curve. $x_i\in R$ is the coordinate of the the i^{th} knot, $x_i\le x_{i+1}$, and n is the number of basis functions which the B-spline comprise. If the knots are equally spaced, the knot vector is called uniform. More than one

knot can be located at the same coordinate and these are referred to as repeated knots. In general, the basis function of order p possesses $p-1$ continuous derivatives. If a knot is repeated k times, than the number of continuous derivatives decreases by k. When a knot is repeated p times, the basis function is interpolatory, but in general, they are not. More about B-spline curves can be found in [20].

B-spline basis functions are defined recursively. For $p=0$, they are constant and expressed as

$$N_{i,0}(x)=\begin{cases}1 & if\ x_i \le x < x_{i+1}\\ 0 & otherwise\end{cases} \quad . \tag{12}$$

For $p=1,2,3,...$, they are defined by

$$N_{i,p}(x)=\frac{x-x_i}{x_{i+p}-x_i}N_{i,p-1}(x)+\frac{x_{i+p+1}-x}{x_{i+p+1}-x_{i+1}}N_{i+1,p-1}(x) \ . \tag{13}$$

The important properties of B-spline basis functions are that they constitute a partition of unity, $\sum_{i=1}^{n} N_{i,p}(x)=1, \ \forall\, x$, and that they are non-negative, i.e. $N_{i,p}(x)\ge 0, \ \forall\, x$.

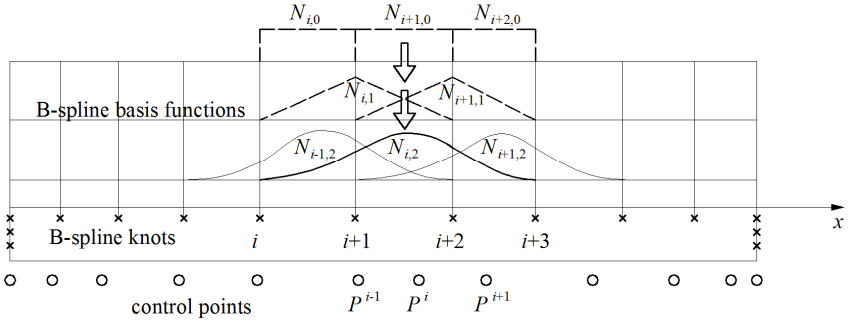

Fig. 2 B-spline basis function computational scheme

A scheme for the derivation of a second order basis function is presented in Fig. 2. As evident, the basis function $N_{i,2}$ is constructed by means of the two first order basis functions $N_{i,1}$ and $N_{i+1,1}$, where each of those is derived by the two functions $N_{i,0}$, $N_{i+1,0}$ and $N_{i+1,0}$, $N_{i+2,0}$, respectively, according to the De Boor–Cox algorithm [21].

B-spline surface is defined as the rectangular tensor product of B-spline curves. Accordingly, the B-spline surface of (p x q)$^{\text{th}}$ order is described by the relation

$$S(x,y)=\sum_{i=1}^{n}\sum_{j=1}^{m} N_{i,p}(x)\, M_{j,q}(y) P_{i,j} \ , \tag{14}$$

where $N_{i,p}(x)$ and $M_{j,q}(y)$ are the basis functions of the B-spline curves of order p and q in the x and y directions, respectively. $P_{i,j}$ are the control points building up the two dimensional control net. Now, the knot vectors are $\mathbf{X}_k=\begin{bmatrix} x_1 & x_2 & \cdots & x_{n+p+1}\end{bmatrix}$ and $\mathbf{Y}_k=\begin{bmatrix} y_1 & y_2 & \cdots & y_{n+q+1}\end{bmatrix}$.

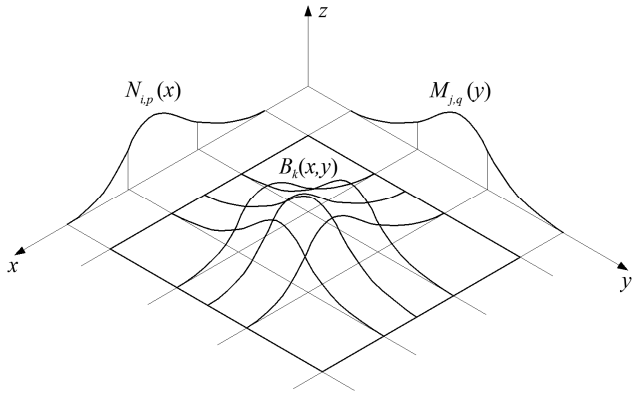

Fig. 3 Construction scheme of a 2-D B-spline basis function

The construction of the B-spline surface over a patch defined by the basis functions $N_{i,p}(x)$ and $M_{j,q}(y)$ is presented in Fig. 3.

According to the above consideration, an in-plane distribution of a variable φ over the defined control points $P_k = P_{i,j}$ may be expressed as the B-spline surface, which can be written in the following form

$$\varphi(\mathbf{X}) = \sum_{k=1}^{n_K} B_k(\mathbf{X})\, P_k = \mathbf{B}(\mathbf{X})\,\mathbf{P}\,, \tag{15}$$

where the abbreviations $\varphi(\mathbf{X}) \equiv S(x,y)$. $B_k(\mathbf{X}) = N_{i,p}(x)\, M_{j,q}(y)$ denotes a 2-D basis function constructed over a patch defined by the functions $N_{i,p}(x)$ and $M_{j,q}(y)$ as presented in Fig. 3. The values of $B_k(\mathbf{X})$ and P_k are expressed in the matrix form as $\mathbf{B}(\mathbf{X})$ and $\mathbf{P}$, respectively. n_K stands for the total number of control points.

Since the B-spline surface is not interpolatory over the control points, the following condition is imposed

$$\mathbf{B}(\mathbf{X}_I)\,\mathbf{P} = \hat{\boldsymbol{\varphi}}_I\,, \tag{16}$$

where $\hat{\boldsymbol{\varphi}}_I$ is the value of φ to be interpolated at the control point $\mathbf{X}_I$. To impose the interpolatory condition, a linear transformation from the fictitous nodal values to the true nodal values should be performed similarly to the transformation found in [3]. Accordingly, the relation of $\mathbf{P} = \mathbf{B}^{-1}(\mathbf{X}_I)\hat{\boldsymbol{\varphi}}_I$ can be easily expressed from (16), and after inserting in (15), the following expression is obtained

$$\varphi(\mathbf{X}) = \mathbf{B}(\mathbf{X})\,\mathbf{B}^{-1}(\mathbf{X}_I)\hat{\boldsymbol{\varphi}}_I = \phi_I(\mathbf{X})\hat{\boldsymbol{\varphi}}_I\,, \tag{17}$$

which yields the B-spline shape function

$$\phi_I(\mathbf{X}) = \mathbf{B}(\mathbf{X})\,\mathbf{B}^{-1}(\mathbf{X}_I)\,, \tag{18}$$

having the Kronecker delta property $\phi_I(\mathbf{X}_J) = \delta_{IJ}$.

3.3 Discretization of governing equations

The stress tensor components in equation (6) are approximated in the in-plane directions by means of the basis functions $\phi_J(\mathbf{X}) = \phi_J\left(X^\delta\right)$ derived above. The linear distribution of the in-plane stress components and the transversal normal stress component over the thickness

is assumed, while the transversal shear stress components are used as constant in the thickness direction. Accordingly, the stress tensor may be expressed in terms of nodal values using the matrix symbols as

$$\boldsymbol{\sigma} = \sum_{J=1}^{n} \boldsymbol{\Phi}_J^{\sigma}\left(\mathbf{X}\right)\hat{\boldsymbol{\sigma}}_J \,, \tag{19}$$

where $\boldsymbol{\sigma}^T = \left[\sigma_{11} \;\; \sigma_{22} \;\; \sigma_{33} \;\; \sigma_{12} \;\; \sigma_{23} \;\; \sigma_{31}\right]$ is the stress vector, $\boldsymbol{\Phi}_J^{\sigma}\left(\mathbf{X}\right)$ is the three-dimensional stress shape function, while the vector $\hat{\boldsymbol{\sigma}}_J$ denotes the nodal stress values

$$\boldsymbol{\Phi}_J^{\sigma}\left(\mathbf{X}\right) = \phi_J\left(X^{\delta}\right)\begin{bmatrix} \alpha\left(X^3\right)\mathbf{I}_4 & \beta\left(X^3\right)\mathbf{I}_4 & \mathbf{0} \\ \mathbf{0} & \mathbf{0} & \mathbf{I}_2 \end{bmatrix} \tag{20}$$

$$\hat{\boldsymbol{\sigma}}_J^T = \left[\hat{\sigma}_{11(l)} \;\; \hat{\sigma}_{22(l)} \;\; \hat{\sigma}_{33(l)} \;\; \hat{\sigma}_{12(l)} \;\; \hat{\sigma}_{11(u)} \;\; \hat{\sigma}_{22(u)} \;\; \hat{\sigma}_{33(u)} \;\; \hat{\sigma}_{12(u)} \;\; \hat{\sigma}_{23(0)} \;\; \hat{\sigma}_{31(0)}\right]_J \tag{21}$$

In the above relations, $\alpha\left(X^3\right)$ and $\beta\left(X^3\right)$ are expressed by (7), while $\mathbf{I}_4$ and $\mathbf{I}_2$ stand for the 4x4 and 2x2 identity matrices, respectively. The notation (*l*) and (*u*) in the subscripts of the vector components (21) describe the values associated with the lower and upper nodes, respectively, and (0) refers to the middle surface. It should be stressed that $\phi_J\left(X^{\delta}\right)$ is the in-plane shape function associated with the J^{th} node couple inside the domain of definition of the current point X^{δ}. Thereby, the domain of definition is a region that includes all nodes whose nodal shape functions do not vanish at the current point, as defined in [22]. n stands for the total number of the node couples inside the domain of definition.

Substituting the approximated stress tensor components from (19) into (6), the discretized governing equations for a local sub-domain surrounding the I^{th} node couple are obtained, which may be written in the matrix form as

$$\begin{aligned}
&\sum_{J=1}^{N_I}\left[\int_{\Omega_s^I}\mathbf{H}(\alpha)\,\boldsymbol{\Phi}_J^{\sigma}\,\mathrm{d}\Omega - \int_{L_s^I}\mathbf{G}(\alpha)\,\mathbf{N}\boldsymbol{\Phi}_J^{\sigma}\,\mathrm{d}\Gamma - \int_{\Gamma_{su}^I}\mathbf{G}(\alpha)\,\mathbf{N}\boldsymbol{\Phi}_J^{\sigma}\,\mathrm{d}\Gamma\right]\hat{\boldsymbol{\sigma}}_J = \\
&\qquad = \int_{\Gamma_{st}^I}\mathbf{G}(\alpha)\,\overline{\mathbf{t}}\,\mathrm{d}\Gamma + \int_{\Omega_s^I}\mathbf{G}(\alpha)\,\mathbf{b}\,\mathrm{d}\Gamma \\
&\sum_{J=1}^{N_I}\left[\int_{\Omega_s^I}\mathbf{H}(\beta)\,\boldsymbol{\Phi}_J^{\sigma}\,\mathrm{d}\Omega - \int_{L_s^I}\mathbf{G}(\beta)\,\mathbf{N}\boldsymbol{\Phi}_J^{\sigma}\,\mathrm{d}\Gamma - \int_{\Gamma_{su}^I}\mathbf{G}(\beta)\,\mathbf{N}\boldsymbol{\Phi}_J^{\sigma}\,\mathrm{d}\Gamma\right]\hat{\boldsymbol{\sigma}}_J = \\
&\qquad = \int_{\Gamma_{st}^I}\mathbf{G}(\beta)\,\overline{\mathbf{t}}\,\mathrm{d}\Gamma + \int_{\Omega_s^I}\mathbf{G}(\beta)\,\mathbf{b}\,\mathrm{d}\Gamma
\end{aligned} \tag{22}$$

with $\mathbf{N}$ as the matrix of the components of the outward unit normal vector $\mathbf{n} = n_i\,\mathbf{e}_i$ on the local sub-domain boundary, and $\mathbf{G}(\alpha) = \alpha(X^3)\mathbf{I}_3$, $\mathbf{G}(\beta) = \beta(X^3)\mathbf{I}_3$ are the diagonal matrices with $\mathbf{I}_3$ as the 3x3 identity matrix. The matrices $\mathbf{H}(\alpha)$, $\mathbf{H}(\beta)$ are computed by the relations

$$\mathbf{H}(\alpha) = \left[\mathbf{D}_k\mathbf{G}(\alpha)\right]^T, \;\; \mathbf{H}(\beta) = \left[\mathbf{D}_k\mathbf{G}(\beta)\right]^T \tag{23}$$

where $\mathbf{D}_k$ stands for the standard 3-D kinematic operator. In addition, in equation (22), N_I denotes the total number of the node couples inside the domain of influence of the I^{th} node

couple. The domain of influence is a region that covers all nodes whose shape functions do not vanish in the local sub-domain surrounding the current node couple. From the discretized equations in (22), it is obvious that there are altogether ten nodal unknowns per each node couple, as expressed in (21). However, the discretized equations represent only six equations for each local sub-domain. Therefore, in order to reduce the overall number of unknowns, the nodal stress components should be expressed in terms of the independently approximated displacements, as described in the following consideration.

The displacement vector $\mathbf{u}^T = \begin{bmatrix} u_1 & u_2 & u_3 \end{bmatrix}$ is expressed in terms of the nodal values by analogy to the above stress interpolation equation as

$$\mathbf{u} = \sum_{K=1}^{n} \mathbf{\Phi}_K^u \left(\mathbf{X} \right) \hat{\mathbf{v}}_K , \tag{24}$$

where the displacement shape function matrix $\mathbf{\Phi}_K^u \left(\mathbf{X} \right)$ is given by

$$\mathbf{\Phi}_K^u \left(\mathbf{X} \right) = \phi_K \left(X^\delta \right) \begin{bmatrix} \alpha\left(X^3\right) & 0 & 0 & \beta\left(X^3\right) & 0 & 0 & 0 \\ 0 & \alpha\left(X^3\right) & 0 & 0 & \beta\left(X^3\right) & 0 & 0 \\ 0 & 0 & \alpha\left(X^3\right) & 0 & 0 & \beta\left(X^3\right) & \gamma\left(X^3\right) \end{bmatrix} \tag{25}$$

Here, besides the linear interpolation of the in-plane displacement components over the thickness described by $\alpha\left(X^3\right)$ and $\beta\left(X^3\right)$, the quadratic hierarchical distribution of the transversal displacement component expressed by

$$\gamma\left(X^3\right) = \frac{1}{2} - 2\left(\frac{X^3}{h} \right)^2 \tag{26}$$

is introduced. Using the quadratic interpolation for the transversal displacement, the undesired thickness locking effect will be overcome. More about this locking phenomenon can be found in [10]. The vector of the unknown variable $\hat{\mathbf{v}}_K$ is

$$\hat{\mathbf{v}}_K^T = \begin{bmatrix} \hat{u}_{1(l)} & \hat{u}_{2(l)} & \hat{u}_{3(l)} & \hat{u}_{1(\mathrm{u})} & \hat{u}_{2(\mathrm{u})} & \hat{u}_{3(\mathrm{u})} & \lambda \end{bmatrix}, \tag{27}$$

where λ is the parameter associated with the quadratic term of the transversal displacement approximation.

By means of the standard 3-D kinematic relation for the strain vector $\boldsymbol{\varepsilon} = \mathbf{D}_k \, \mathbf{u}$ and the constitutive equation $\boldsymbol{\sigma} = \mathbf{D}\boldsymbol{\varepsilon}$, where $\mathbf{D}$ stands for the 3-D elasticity stress-strain matrix, the nodal stress vector may be expressed in terms of the nodal values $\hat{\mathbf{v}}_K$ as

$$\hat{\boldsymbol{\sigma}}_J = \sum_{K=1}^{n_J} \tilde{\mathbf{B}}_{KJ} \hat{\mathbf{v}}_K , \tag{28}$$

where $\tilde{\mathbf{B}}_{KJ} = \mathbf{D}\,\mathbf{B}_K \left(\mathbf{X}_J \right)$ with $\mathbf{B}_K \left(\mathbf{X}_J \right)$ as the matrix containing derivatives of the 3-D displacement shape function matrix. n_J is the total number of the node couples inside the domain of definition of the J^{th} node couple. After inserting equation (28) into (22) and by neglecting the terms containing the body force vector, the following final discretized form of the governing equations on the domain of influence level is obtained

$$\sum_{J=1}^{N_I}\left[\int_{\Omega_s^I}\mathbf{H}(\alpha)\,\boldsymbol{\Phi}_J^{\sigma}\,\mathrm{d}\Omega-\int_{L_s^I}\mathbf{G}(\alpha)\,\mathbf{N}\boldsymbol{\Phi}_J^{\sigma}\,\mathrm{d}\Gamma-\int_{\Gamma_{su}^I}\mathbf{G}(\alpha)\,\mathbf{N}\boldsymbol{\Phi}_J^{\sigma}\,\mathrm{d}\Gamma\right]\sum_{K=1}^{n_J}\tilde{\mathbf{B}}_{KJ}\hat{\mathbf{v}}_K=$$
$$=\int_{\Gamma_{st}^I}\mathbf{G}(\alpha)\,\bar{\mathbf{t}}\,\mathrm{d}\Gamma$$
$$\sum_{J=1}^{N_I}\left[\int_{\Omega_s^I}\mathbf{H}(\beta)\,\boldsymbol{\Phi}_J^{\sigma}\,\mathrm{d}\Omega-\int_{L_s^I}\mathbf{G}(\beta)\,\mathbf{N}\boldsymbol{\Phi}_J^{\sigma}\,\mathrm{d}\Gamma-\int_{\Gamma_{su}^I}\mathbf{G}(\beta)\,\mathbf{N}\boldsymbol{\Phi}_J^{\sigma}\,\mathrm{d}\Gamma\right]\sum_{K=1}^{n_J}\tilde{\mathbf{B}}_{KJ}\hat{\mathbf{v}}_K=\tag{29}$$
$$=\int_{\Gamma_{st}^I}\mathbf{G}(\beta)\,\bar{\mathbf{t}}\,\mathrm{d}\Gamma$$

As obvious from (29), six equations are generated for each local sub-domain, while there are seven unknowns at each node, including the six nodal displacement components at the nodes on the upper and lower surface and the parameter λ associated with the quadratic term of the transversal displacement interpolation. Therefore, additional equations are required for the solution of the boundary value problem.

To obtain the additional equations, the equilibrium in the transversal direction is enforced at the mid-points located on the middle surface within each local sub-domain. Accordingly, the equilibrium at the mid-point $\mathbf{X}_{(0)}^I$, as shown in Fig. 4, is expressed by the relation

$$\sigma_{3j,j}\left(\mathbf{X}_{(0)}^I\right)+b_3\left(\mathbf{X}_{(0)}^I\right)=0\,. \tag{30}$$

After the discretization procedure described above and the omitting of the body force, the following additional equation is obtained

$$\sum_{J=1}^{n_I}\Big[0\quad 0\quad -\frac{1}{h}\phi_J\left(X^{\delta}\right)\quad 0\quad \phi_{J,X^2}\left(X^{\delta}\right)\quad \phi_{J,X^1}\left(X^{\delta}\right)$$
$$0\quad 0\quad \frac{1}{h}\phi_J\left(X^{\delta}\right)\quad 0\Big]\sum_{K=1}^{n_J}\tilde{\mathbf{B}}_{KJ}\hat{\mathbf{v}}_K=0 \tag{31}$$

Herein, n_I is the total number of the node couples inside the domain of definition of the I^{th} node couple. Now, for each local sub-domain, a system of seven equations, expressed by (29) and (31), with seven unknowns, is derived. For the domain of influence with N couple of nodes, a set of $7N$ equations with the equal number of unknowns is evaluated. A closed global system of equations on the structural level is derived by using the node-by-node numerical assemblage procedure.

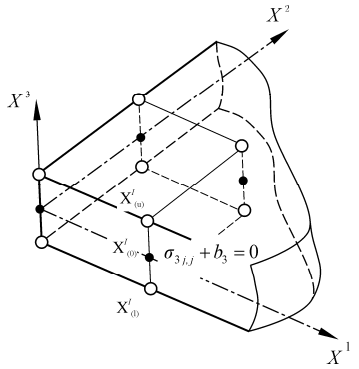

Fig. 4 Mid-point equilibrium for the elimination of thickness locking effect

From the presented formulation it is clear that, in contrast to the fully displacement meshless formulation, the differentiation of the shape functions over the local sub-domains is avoided, because their derivatives are needed only at the nodes, which should contribute to the stability and accuracy of numerical solutions. Due to the stress interpolation scheme, the shear locking effect should be completely suppressed as will be demonstrated by the following numerical examples.

4. Numerical examples

4.1 Thin cantilever plate under transversal line load at free end

As the first example, the bending of a cantilever plate subjected to the transversal line load of $q = 100 \cdot h^3$ is considered. The length and the width of the plate are $l = 10$ and $b = 1$, as shown in Fig. 5. The material data are Young's modulus $E = 200000$ and Poisson's ratio $\nu = 0.0$. The plate is discretized by uniformly distributed grid points on the upper and lower surface in the directions of the global axes X^1 and X^2.

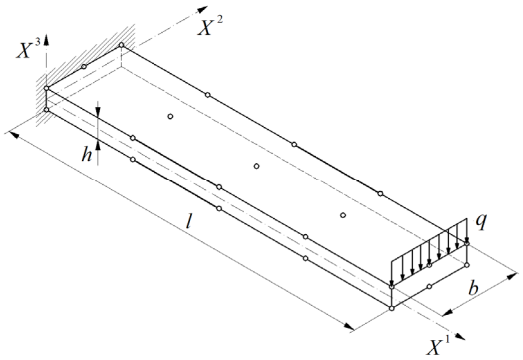

Fig. 5 Cantilever plate under transversal load

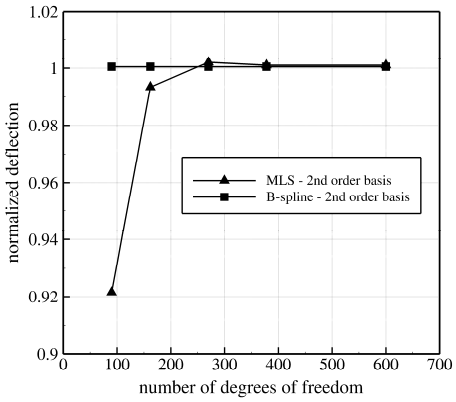

Fig. 6 Convergence of free end deflection for *l/h* = 100

The results computed by the present formulation using the MLS interpolation with the second order polynomial basis and by means of the biquadratic B-spline shape function are compared in Fig. 6, presenting the convergence study. The plate length to thickness ratio is $l / h = 100$ and the free end deflection is normalized by using the exact analytical solution [23]. As evident, the exact solution is achieved with fewer degrees of freedom when the B-spline interpolation is used.

A more detailed convergence study employing the relative deflection error in the discrete L_2 norm has been performed. The results obtained by using both the MLS and the B-spline shape functions are again compared in Fig. 7. The relative error is defined as

$$r_w = \sqrt{\frac{\sum_{I=1}^{N}\left(u_i^I - u_i^{aI}\right)^2}{\sum_{I=1}^{N}\left(u_i^{aI}\right)^2}}, \tag{32}$$

where u_i^I is the result of the meshless computation and u_i^{aI} stands for the exact analytical solution at the nodes.

As may be seen, the formulation using the B-spline shape function is much more accurate for relatively coarse discretizations, but the accuracy is decreased for large numbers

of degrees of freedom. Furthermore, it was noticed during the computations that the loss of accuracy was accompanied by an increase in the condition number of the global stiffness matrix, which could be a reason for the loss of accuracy. The ill-conditioning of the global coefficient matrix may be caused by the linear transformation from the fictitous nodal parameters to the true nodal values presented in (17), performed in order to impose the nodal point interpolation.

The sensitivity of the proposed mixed approach to the shear locking effect has been tested by increasing the plate span to thickness ratio, as displayed in Fig. 8. As obvious, the convergence is achieved even for very thin plates by both interpolation functions, which shows that the shear locking effect is completely eliminated.

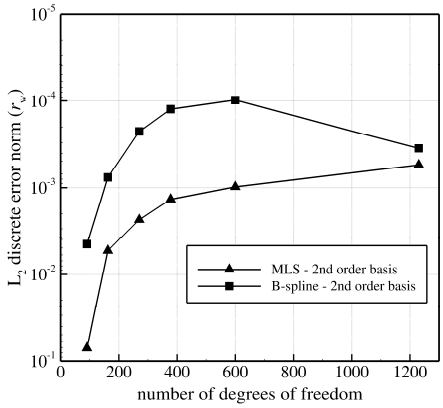

Fig. 7 Relative errors of plate deflection for *l/h*=100

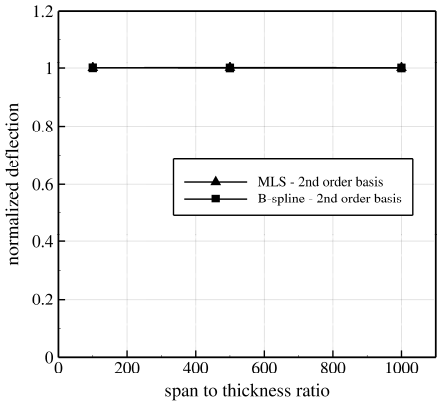

Fig. 8 Free end plate deflection vs. span to thickness ratio for cantilever plate

4.2 Clamped thin square plate under uniform load

As the second example, a clamped thin square plate under the uniformly distributed load of $q = 0.001$ is analyzed. The plate thickness to span ratio is $h / a = 0.01$ and the material data are Young's modulus $E = 200000$ and Poisson's ratio $\nu = 0.3$. Due to symmetry, only one quarter of the plate is discretized by uniformly distributed grid points on the upper and lower surface. The discretization over the plate surface by 5x5 nodes is shown in Fig. 9.

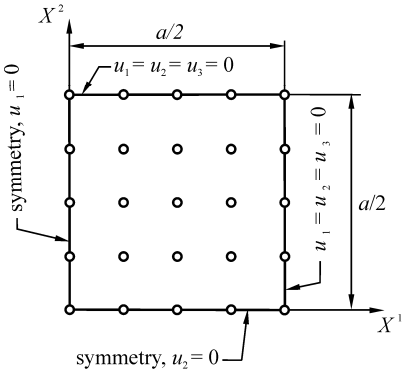

Fig. 9 Discretization and boundary conditions of clamped plate

The relative deflection error in the L_2 norm expressed by (32) has again been calculated and the results obtained by the MLS and B-spline shape functions are compared in Fig. 10. As evident from the figure and like in the previous example, the formulation using the B-spline interpolation exhibits better accuracy for the discretization with a small number of degrees of freedom. However, the advantage of the B-spline again disappears in the case of a very fine discretization.

Now, by analogy to the previous example, the sensitivity of the proposed formulation to the shear locking effect has been tested by increasing the span to thickness ratio and the results are shown in Fig. 11. As evident, the shear locking is suppressed again.

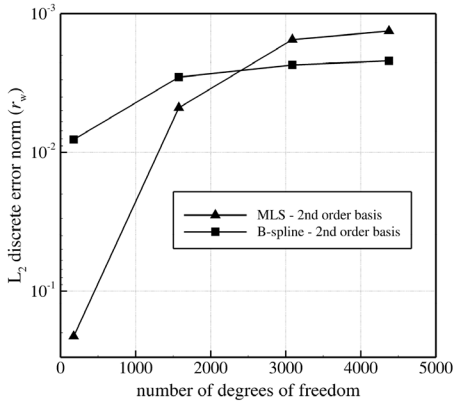

Fig. 10 Relative errors of clamped plate deflection

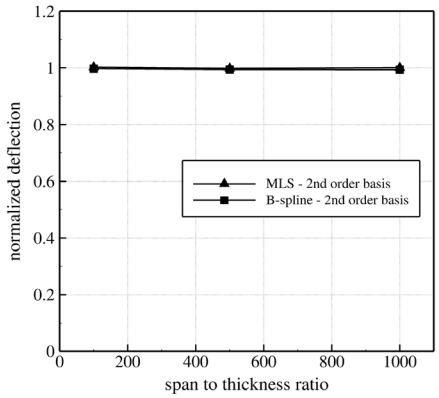

Fig. 11 Central deflection vs. span to thickness ratio for clamped plate under uniform load

5. Conclusion

A new mixed meshless Local Petrov-Galerkin formulation employing both the stress and the displacement interpolations has been proposed for the analysis of plate structures. The kinematic of a 3-D solid is applied, allowing the use of complete 3-D constitutive equations. The interpolation has been performed by using the MLS and the B-spline shape functions in the in-plane directions, while the simple polynomials are used for the interpolation over the thickness. In order to eliminate the thickness locking effect, the hierarchical quadratic interpolation of the transversal displacement component through the thickness has been applied. The shear locking is completely eliminated by means of the stress interpolation. In contrast to the mixed meshless formulations already proposed by the authors, the complex transformations employed in the strain and the stress description are avoided in the formulation presented.

The results computed by the present formulation using the MLS and the B-spline shape functions are compared. Both interpolation strategies exhibit accurate solutions, and the locking phenomena are completely suppressed, as shown by the numerical examples. The formulation using B-spline shape function yields smaller errors at a relatively coarse grid point distribution, but accuracy is reduced in the case of a very fine discretization. Furthermore, the derivation procedure of the B-spline shape function is much simpler than that of the MLS formulation, which is advantageous in meshless analyses.

The reason for the loss of accuracy at the large number of degrees of freedom may be the ill-conditioned global coefficient matrix, which appears due to the linear transformation used to impose the interpolatory condition of the B-spline shape function. Therefore, further research is required to avoid the ill-conditioning of the global matrix arising because of the mentioned transformation procedure. In addition, other more efficient strategies to obtain the B-spline interpolation function with the Kronecker delta property should be considered.

REFERENCES

[1] P. Krysl, T. Belytschko, Analysis of thin shells by the Element-Free Galerkin method, International Journal of Solids and Structures, 33 (1996) 3057-3080.

[2] H. Noguchi, T. Kawashima, T. Miyamura, Element free analyses of shell and spatial structures, International Journal for Numerical Methods in Engineering, 47 (2000) 1215-1240.

[3] S.N. Atluri, The Meshless Method (MLPG) for Domain & BIE Discretization, Tech Science Press, Forsyth, USA, 2004.

[4] S. Long, S.N. Atluri, A Meshless Local Petrov-Galerkin Method for Solving the Bending Problem of a Thin Plate, CMES: Computer Modeling in Engineering & Sciences, 3 (2002) 53-63.

[5] D.F. Gilhooley, R.C. Batra, J.R. Xiao, M.A. McCarthy, J.W. Gillespie Jr, Analysis of thick functionally graded plates by using higher-order shear and normal deformable plate theory and MLPG method with radial basis functions, Composite Structures, 80 (2007) 539-552.

[6] J. Sladek, V. Sladek, H.A. Mang, Meshless LBIE formulations for simply supported and clamped plates under dynamic load, Computers & Structures, 81 (2003) 1643-1651.

[7] L.F. Qian, R.C. Batra, L.M. Chen, Static and dynamic deformations of thick functionally graded elastic plates by using higher-order shear and normal deformable plate theory and meshless local Petrov-Galerkin method, Composites Part B: Engineering, 35 (2004) 685-697.

[8] J. Sladek, V. Sladek, P.H. Wen, M.H. Aliabadi, Meshless Local Petrov-Galerkin (MLPG) Method for Shear Deformable Shells Analysis, CMES: Computer Modeling in Engineering & Sciences, 13 (2006) 103-117.

[9] J. Sladek, V. Sladek, J. Krivacek, M.H. Aliabadi, Local boundary integral equations for orthotropic shallow shells, International Journal of Solids and Structures, 44 (2007) 2285-2303.

[10] J. Soric, Q. Li, T. Jarak, S.N. Atluri, Meshless local Petrov-Galerkin (MLPG) formulation for analysis of thick plates, CMES: Computer Modeling in Engineering & Sciences, 6 (2004) 349-357.

[11] Q. Li, J. Soric, T. Jarak, S.N. Atluri, A locking-free meshless local Petrov-Galerkin formulation for thick and thin plates, Journal of Computational Physics, 208 (2005) 116-133.

[12] T. Jarak, J. Soric, J. Hoster, Analysis of shell deformation responses by the meshless local Petrov-Galerkin (MLPG) approach, CMES: Computer Modeling in Engineering & Sciences, 18 (2007) 235-246.

[13] T. Jarak, J. Soric, Analysis of rectangular square plates by the mixed Meshless Local Petrov-Galerkin (MLPG) approach, CMES: Computer Modeling in Engineering & Sciences, 38 (2008) 231-261.

[14] J. Soric, T. Jarak, Mixed meshless formulation for analysis of shell-like structures, Computer Methods in Applied Mechanics and Engineering, 199 (2010) 1153-1164.

[15] T. Most, C. Bucher, A Moving Least Squares weighting function for the Element-free Galerkin Method which almost fulfills essential boundary conditions, Structural Engineering and Mechanics, 21 (2005) 315-332.

[16] T. Most, A natural neighbour-based moving least-squares approach for the element-free Galerkin method, International Journal for Numerical Methods in Engineering, 71 (2007) 224-252.

[17] S.N. Atluri, T.-L. Zhu, The meshless local Petrov-Galerkin (MLPG) approach for solving problems in elasto-statics, Computational Mechanics, 25 (2000) 169-179.

[18] G.R. Liu, Mesh Free Methods: Moving beyond the Finite Element Method, CRC Press, Boca Raton,USA., 2003.

[19] H.Y. Roh, M. Cho, Integration of geometric design and mechanical analysis using B-spline functions on surface, International Journal for Numerical Methods in Engineering, 62 (2005) 1927-1949.

[20] J.A. Cottrell, T.J.R. Hughes, Y. Bazilevs, Isogeometric Analysis: Toward Integration of CAD and FEA, John Wiley & Sons, Ltd., Singapore, 2009.

[21] L. Piegl, W. Tiller, The NURBS Book, Springer, Berlin, 1997.

[22] S.N. Atluri, T.-L. Zhu, A new Meshless Local Petrov-Galerkin (MLPG) approach in computational mechanics, Computational Mechanics, 22 (1998) 117-127.

[23] S. Timoshenko, S. Voinowsky-Krieger, Theory of Plates and Shells, McGraw-Hill, London, 1985.

Submitted: 01.7.2014

Accepted: 04.3.2015

Jurica Sorić
Tomislav Jarak
Boris Jalušić
University of Zagreb
Faculty of Mechanical Engineering and Naval Architecture
Ivana Lučića 5, 10000 Zagreb, Croatia
Josip Hoster
Karlovac University of Applied Sciences
Ivana Meštrovića 10, 47000 Karlovac, Croatia